

# Impact of ultraluminous X-ray sources on photoabsorption in the first galaxies

S. Sazonov<sup>1,2★</sup> and I. Khabibullin<sup>3,1</sup>

<sup>1</sup>*Space Research Institute, Russian Academy of Sciences, Profsoyuznaya 84/32, 117997 Moscow, Russia*

<sup>2</sup>*Moscow Institute of Physics and Technology, Institutskiy per. 9, 141700 Dolgoprudny, Russia*

<sup>3</sup>*Max Planck Institute for Astrophysics, Karl-Schwarzschild-Strasse 1, D-85741 Garching, Germany*

5 February 2018

## ABSTRACT

In the local Universe, integrated X-ray emission from high-mass X-ray binaries (HMXBs) is dominated by the brightest ultraluminous X-ray sources (ULXs) with luminosity  $\gtrsim 10^{40}$  erg s<sup>-1</sup>. Such rare objects probably also dominated the production of X-rays in the early Universe. We demonstrate that a ULX with  $L_X \sim 10^{40}–10^{41}$  erg s<sup>-1</sup> (isotropic-equivalent luminosity in the 0.1–10 keV energy band) shining for  $\sim 10^5$  years (the expected duration of a supercritically accreting phase in HMXBs) can significantly ionise the ISM in its host dwarf galaxy of total mass  $M \sim 10^7–10^8 M_\odot$  and thereby reduce its opacity to soft X-rays. As a result, the fraction of the soft X-ray (below 1 keV) radiation from the ULX escaping into the intergalactic medium (IGM) can increase from  $\sim 20–50\%$  to  $\sim 30–80\%$  over its lifetime. This implies that HMXBs can induce a stronger heating of the IGM at  $z \gtrsim 10$  compared to estimates neglecting the ULX feedback on the ISM. However, larger galaxies with  $M \gtrsim 3 \times 10^8 M_\odot$  could not be significantly ionised even by the brightest ULXs in the early Universe. Since such galaxies probably started to dominate the global star-formation rate at  $z \lesssim 10$ , the overall escape fraction of soft X-rays from the HMXB population probably remained low,  $\lesssim 30\%$ , at these epochs.

**Key words:** stars: black holes – accretion, accretion discs – X-rays: binaries – X-rays: ISM – galaxies: high-redshift – dark ages, reionization, first stars

## 1 INTRODUCTION

Already by  $z \sim 10$ , i.e. significantly before the Universe was completely reionised (by  $z \sim 6$ ), the intergalactic medium (IGM) may have been heated above the temperature of the cosmic microwave background (CMB),  $T_{\text{CMB}} = 2.726(1+z)$  K, by photoionising radiation from the first generations of X-ray sources (e.g. Venkatesan, Giroux, & Shull 2001; Madau et al. 2004; Ricotti & Ostriker 2004; Mirabel et al. 2011)<sup>1</sup>. High-mass X-ray binaries (HMXBs) probably played the main role in this process, and many authors have estimated the expected IGM temperature increment and the associated 21 cm signal from the early Universe (most recently, Madau & Fragos 2017; Sazonov & Khabibullin 2017a; Ross et al. 2017; Cohen et al. 2017). These predictions are important for preparing to 21 cm observations of the reionisation

epoch by upcoming experiments such as the Square Kilometer Array (SKA<sup>2</sup>).

Apart from the fairly uncertain specific (i.e. per unit star formation rate, SFR) X-ray emissivity of HMXBs in the first galaxies, another poorly known aspect of the problem is whether the soft X-rays emitted by HMXBs were actually able to escape into the IGM through the interstellar medium (ISM) of their host galaxies. This is important because only X-ray photons with energies  $E \lesssim 1$  keV could efficiently heat the Universe at  $z \lesssim 20$ , as the IGM was essentially transparent to harder X-ray radiation. Recently, Das et al. (2017) used high-resolution simulations of dwarf galaxies at  $z > 7$  (Wise et al. 2014), taking into account radiative and supernova feedback from massive metal-free (Population III) and metal enriched stars on the ISM, to estimate neutral hydrogen column densities through the host galaxies of HMXBs. These proved to vary widely (by 1–2 orders of magnitude) from one line of sight to another and between different galaxies, with median values of  $N_{\text{H}} \sim 3 \times 10^{21}$  cm<sup>-2</sup>. Such column

★ E-mail: sazonov@iki.rssi.ru

<sup>1</sup> as well as by low-energy cosmic rays from the first supernovae (Sazonov & Sunyaev 2015; Leite et al. 2017) and microquasars (Tueros, del Valle, & Romero 2014; Douma et al. 2017)

<sup>2</sup> <https://www.skatelescope.org>

densities (in the essentially metal-free medium of the first galaxies) imply that the soft X-ray emission from HMXBs should be attenuated by photoabsorption in their host galaxies by more than a factor of 3 at  $E < 500$  eV, significantly weakening the X-ray heating of the IGM in the early Universe. Note that [Das et al. \(2017\)](#) assumed all helium (and heavier elements) in the ISM to be neutral, while helium is the main photoabsorbing agent of soft X-rays in a metal-poor medium.

Virtually all previous studies were based on the assumption that HXMB X-ray emissivity is proportional to the SFR. Although this conjecture is certainly reasonable when averaging over a large ensemble of galaxies, it fails when considering galaxies individually. Statistical studies of HMXBs and ultraluminous X-ray sources (ULXs, usually defined as point-like, off-nucleus sources with luminosity  $\gtrsim 10^{39}$  erg s $^{-1}$ ) in large samples of nearby galaxies have demonstrated that the summed X-ray emission of HMXBs and ULXs in the local Universe is dominated by the brightest sources with luminosity  $\gtrsim 10^{40}$  erg s $^{-1}$  ([Mineo, Gilfanov, & Sunyaev 2012](#)) or perhaps even  $\sim 10^{41}$  erg s $^{-1}$  (sometimes referred to as hyperluminous X-ray sources, HLXs), as the measured *intrinsic* HMXB/ULX X-ray luminosity function (LF) continues with a slope  $\alpha \sim 0.6$  ( $dN/d\log L \propto L^{-\alpha}$ ) up to  $\sim 10^{40.5}$  erg s $^{-1}$  (in the 0.25–8 keV energy band, and the same slope pertains to the LF measured in the softer band of 0.25–2 keV), with no reliably detected cutoff ([Sazonov & Khabibullin 2017b](#)). Recent studies indicate that the majority of ULXs are an extension of the HMXB population towards higher, supercritical accretion rates onto neutron stars and stellar-mass black holes (see [Kaaret, Feng, & Roberts 2017](#) for a recent review), rather than accreting intermediate-mass black holes.

Although ULXs dominate the total X-ray output of HMXBs, such objects are rare. Specifically, there are just  $\sim 1.45$  ( $\sim 0.36$ ) sources with luminosity (absorption corrected, 0.25–8 keV) more than  $10^{39}$  ( $10^{40}$ ) erg s $^{-1}$  per a SFR of  $1 M_{\odot}$  yr $^{-1}$  in the local Universe ([Sazonov & Khabibullin 2017b](#)), so that many Milky Way sized galaxies do not contain such sources at all (including the Milky Way itself, although the supercritical accretor SS 433 would probably look like a ULX if we were viewing our Galaxy face-on, [Fabrika & Mescheryakov 2001](#); [Begelman, King, & Pringle 2006](#); [Poutanen et al. 2007](#); see, however, [Khabibullin & Sazonov 2016](#) for upper limits on the collimated X-ray emission of SS 433). Assuming that the shape of the HMXB/ULX LF in the early Universe was similar to that at  $z = 0$  and given that the bulk of star formation at  $z \sim 10$  was taking place in dwarf galaxies with typical SFR  $\lesssim 10^{-2} M_{\odot}$  yr $^{-1}$  (e.g. [Xu et al. 2016](#)), ULXs were even rarer objects at those epochs: sources with luminosity  $\gtrsim 10^{40}$  erg s $^{-1}$  were present (at any given time) only in every  $\sim 100$ th galaxy (even taking into account that the specific HMXB occurrence rate was probably higher by a factor of  $\lesssim 10$  due the low metallicity of the first galaxies (e.g. [Brorby, Kaaret, & Prestwich 2014](#); [Douna et al. 2015](#); [Basu-Zych et al. 2016](#); [Lehmer et al. 2016](#)). Nevertheless, the X-ray background in the early Universe was probably dominated by such extremely bright and rare ‘lighthouses’!

Population synthesis modelling of massive binaries suggests that supercritical accretion episodes with the X-ray luminosity reaching  $\sim 10^{40}$ – $10^{41}$  erg s $^{-1}$  can last up to a few  $\times 10^5$  yr ([Rappaport, Podsiadlowski, & Pfahl 2005](#);

[Pavlovskii et al. 2017](#); [Wiktorowicz et al. 2017](#)). If such a ULX shined in a dwarf galaxy, it might significantly photoionise the ambient ISM and thereby reduce the obscuration of its soft X-ray radiation for an extra-galactic observer [there is some similarity here with supersoft X-ray sources (nuclear-burning white dwarfs) photoionising the circumstellar matter around them, [Nielsen & Gilfanov 2015](#)]. In particular, since in a neutral metal-poor medium, X-rays are mostly absorbed by helium atoms, it is possible that a bright ULX will primarily ionise helium rather than hydrogen in the ISM, but that will still substantially weaken the attenuation of the ULX radiation. Eventually, this would cause stronger IGM heating in the early Universe. The goal of the present, proof-of-concept study is to evaluate such ULX radiative feedback on the ISM of the first galaxies.

The following values of cosmological parameters are used below:  $\Omega_m = 0.309$ ,  $\Omega_{\Lambda} = 1 - \Omega_m$ ,  $\Omega_b = 0.049$ ,  $H_0 = 68$  km s $^{-1}$  Mpc $^{-1}$  and  $Y = 0.246$  (helium mass fraction).

## 2 BASIC ASSUMPTIONS

The bulk of star formation in the cosmic X-ray heating epoch under consideration ( $z \sim 12$ – $8$ ) was taking place in minihaloes and haloes with total masses  $\sim 10^7$ – $10^9 M_{\odot}$ , with the lower and higher values in this range being typical of the earlier and later epochs, respectively (e.g. [Xu et al. 2016](#)). Below we consider a situation where a single ULX appears in a star-forming halo and study its photoionisation effect on the gas within the halo.

### 2.1 Properties of the halo and its gas

We consider a spherical dark matter halo of mass  $M$  virialising at redshift  $z$ , and assume that its density follows a Navarro-Frenk-White (NFW) radial profile ([Navarro, Frenk, & White 1997](#)):

$$\rho(r) = \frac{18\pi^2 c^2 \bar{\rho}(z)}{3F(c)x(1+cx)^2}. \quad (1)$$

Here,  $\bar{\rho}(z)$  is the mean matter density of the Universe at redshift  $z$ ,  $x = r/R_{\text{vir}}$ ,  $R_{\text{vir}}$  is the halo virial radius,  $c$  is the concentration parameter and  $F(c) = \ln(1+c) - c/(1+c)$ . We define  $R_{\text{vir}}$  as the radius within which the average density is  $18\pi^2 \approx 178$  times the critical density at the given epoch. For the adopted cosmological parameters,

$$R_{\text{vir}} = 1.5 \left( \frac{M}{10^8 M_{\odot}} \right)^{1/3} \left( \frac{1+z}{10} \right)^{-1} \text{ kpc} \quad (2)$$

([Loeb & Furlanetto 2013](#)).

We adopt  $c = 2$ , since this value of the concentration parameter is expected to be typical in the considered range of (high) redshifts and (small) halo masses ([Pilipenko et al. 2017](#)). Following a number of previous theoretical studies of dwarf galaxies at the beginning of cosmic reionisation (e.g. [Xu, Ferrara, & Chen 2011](#); [Ferrara & Loeb 2013](#)), we assume that the gas in the halo has initial (prior to X-ray irradiation) temperature  $T_0$  and is in hydrostatic equilibrium within the dark matter potential well ([Makino, Sasaki, & Suto 1998](#)):

$$\rho_g = \rho_{g0} e^{-(T_{\text{vir}}/T_0)[v_c^2(0) - v_c^2(r)]/V_c^2}. \quad (3)$$

Here,  $\rho_{g0}$  is the central gas density,  $V_c = (GM/R_{\text{vir}})^{1/2}$  is the circular velocity at the virial radius,  $T_{\text{vir}} = (\mu m_p/2k_B)V_c^2$  is the virial temperature of the halo (where  $\mu$  is the mean molecular weight of the gas,  $m_p$  is the proton mass and  $k_B$  is the Boltzmann constant) and  $v_c(r)$  is the escape velocity at radius  $r$ , given by

$$v_c^2(r) = 2V_c^2 \frac{F(cx) + cx/(1+cx)}{xF(c)}. \quad (4)$$

For the adopted cosmological parameters, the virial temperature is given by (Loeb & Furlanetto 2013)

$$T_{\text{vir}} = 1.0 \times 10^4 \frac{\mu}{0.6} \left( \frac{M}{10^8 M_\odot} \right)^{2/3} \frac{1+z}{10} \text{ K}. \quad (5)$$

Note that it can vary by a factor of 2 depending on the ionisation state of the gas ( $\mu \approx 0.6$  and 1.2 for a fully ionised and neutral gas, respectively).

Equation (3) allows for the possibility that the gas temperature is different from the halo virial temperature. This factor is aimed to crudely reflect the current uncertainty in the morphology of the gas in high-redshift haloes associated with a multitude of physical processes affecting their assembly, such as gas cooling, large-scale motions and turbulence arising during halo virialisation and mergers, angular momentum of the inflowing gas, stellar and supernova feedback etc. Cosmological hydrodynamical simulations suggest that high-redshift dwarf galaxies and minihaloes were quite irregular but their overall morphology was rounder compared to the more massive galaxies at later epochs and most of them probably did not form well-defined central discs (e.g. Wise & Abel 2007; Greif et al. 2008; Wise & Cen 2009; Romano-Díaz et al. 2011; Wise et al. 2014).

From the above formulae, the gas density can finally be expressed as

$$\rho_g(x) = \rho_{g0} e^{-AT_{\text{vir}}/T_0} (1+cx)^{A(T_{\text{vir}}/T_0)/cx}, \quad (6)$$

where  $A = 2c/F(c)$ . The central gas density is determined by equating the total gas fraction within the virial radius,  $f_g \equiv M_g/M$ , to the cosmological value,  $\Omega_b/\Omega_m \approx 0.16$ ; thus

$$\rho_{g0} = \frac{(18\pi^2/3)f_g c^3 e^{AT_{\text{vir}}/T_0}}{\int_0^c t^2 (1+t)^{A(T_{\text{vir}}/T_0)/t} dt} \bar{\rho}(z). \quad (7)$$

Since high-redshift dwarf galaxies and minihaloes were very metal poor, we assume, in our baseline model, the gas to consist of hydrogen and helium in their primordial mass ratio (0.754 to 0.246). However, we have also carried out tests to check the sensitivity of our results to the presence of small amounts of metals in the gas.

We do not consider the gas outside the halo, since its X-ray absorption optical depth is expected to be small. Indeed, since the average hydrogen number density in the Universe  $\langle n_H \rangle \sim 3 \times 10^{-4} [(1+z)/10]^3 \text{ cm}^{-3}$  and the density outside the halo gradually declines from  $\sim 4\langle n_H \rangle$  at  $R_{\text{vir}}$  to less than  $2\langle n_H \rangle$  at a few  $R_{\text{vir}}$  (e.g. Bertschinger 1985; Medvedev, Sazonov, & Gilfanov 2016), the total column density through the IGM outside the halo is  $\lesssim$  a few  $10^{19} (M/10^8 M_\odot)^{1/3} [(1+z)/10]^2 \text{ cm}^{-2}$ , much less than  $N_H \sim 10^{21} - 10^{22} \text{ cm}^{-2}$  expected for the halo itself.

## 2.2 ULX properties

Suppose that a ULX switches on at the centre of the halo (during a cosmologically short star-formation episode) and emits an X-ray luminosity  $L_X$  in the energy range from 100 eV to 10 keV for a time  $t_X$ . We assume that the source's X-ray spectrum has a power-law shape with a photon index  $\Gamma = 2.1$  ( $dN_\gamma/dE \propto E^{-\Gamma}$ ). Such a spectrum fits well the absorption-corrected summed X-ray spectrum of luminous ( $L_X \gtrsim 10^{38} \text{ erg s}^{-1}$ , including ULXs) HMXBs in the local Universe and represents the angle-integrated X-ray emission of the near- and supercritically accreting neutron stars and stellar-mass black holes at  $z=0$  (Sazonov & Khabibullin 2017c).

This spectrum was originally obtained from *Chandra* X-ray Observatory data in the 0.25–8 keV band. Here, we extrapolate it to a somewhat broader energy range, in particular to lower energies, because (i) theoretical models of supercritical accretion (e.g. Watarai et al. 2000; Poutanen et al. 2007; Kawashima et al. 2012; Vinokurov, Fabrika, & Atapin 2013; Narayan, Sądowski, & Soria 2017), (ii) observations of extended (several hundred parsecs) high-ionisation nebulae around ULXs (e.g. Pakull & Mirioni 2003; Kaaret, Ward, & Zezas 2004; Berghea et al. 2010)<sup>3</sup> and (iii) optical/UV observations of the Galactic microquasar SS 433 (Cherepashchuk, Aslanov, & Kornilov 1982; Dolan et al. 1997; Fabrika 2004) suggest that the supercritical disc with an outflowing wind emits at soft X-ray/UV energies a luminosity comparable to the X-ray luminosity emergent from the central disc funnel. Our choice of the value of 100 eV for the lower boundary of the spectral energy range is rather arbitrary and partly driven by the fact that the apparently power-law shape of the aforementioned collective X-ray spectrum of luminous HMXBs (Sazonov & Khabibullin 2017c) results from averaging over very diverse spectra (from hard to supersoft) of individual sources, and it is not obvious how to extrapolate such a summed spectrum substantially below its original lower energy boundary (250 eV). In addition, this choice is motivated by the estimated temperature of the accretion disc's wind in SS 433 of  $T_{\text{wind}} \sim 5 \times 10^4 \text{ K}$  and the expectation (based on a theoretical scaling relation of  $T_{\text{wind}}$  with the supercritical accretion rate) that the winds in typical ULXs may be hotter by a factor of a few, i.e.  $T_{\text{wind}} \lesssim 2 \times 10^5 \text{ K}$  (Fabrika et al. 2015). One may therefore expect a substantial fraction of the X-ray radiation emitted by the supercritical accretion disk to be reprocessed by the wind at energies  $E \sim 4kT_{\text{wind}} \lesssim 100 \text{ eV}$ .

Importantly, the quantity  $L_X$  introduced above is not meant to be the angle-integrated luminosity of the ULX. In fact, the ULX radiation is likely to be collimated along the axis of the supercritical accretion disc (e.g. King 2009) and then by  $L_X$  one should understand an 'isotropic-equivalent luminosity', i.e.  $L_X = 4\pi D^2 f_X$  (where  $D$  is the distance to the source and  $f_X$  is the measured X-ray flux), which would be perceived by an observer viewing the disc nearly face-on. It is this apparent luminosity that is relevant for the present study, since our goal is to explore the photoionisation effect of the ULX on the gas located in front of its X-ray beam,

<sup>3</sup> Some of these nebulae may be close analogs of the ionisation bubbles inflated by ULXs in the first galaxies, discussed in the present study.

which further irradiates the surrounding IGM. In reality, the intensity and spectral shape of the radiation emitted by the ULX is likely to vary with the offset angle from the axis of the disc in a more complicated way, but since this dependence is poorly known and moreover can depend on the accretion rate and the nature of the relativistic compact object (black hole vs. neutron star), we ignore it in our modelling.

The key parameters of the model are thus  $L_X$  and  $t_X$ . To get an idea of how large their values can be, suppose that a ULX is powered by accretion from a stellar companion onto a relativistic compact object, the radiative efficiency of accretion is  $\eta$  and the X-ray radiation is collimated within two opposite cones subtending a total solid angle  $\Omega$ . Then, the total mass accreted from the companion (part of which may be ejected as a wind from the system and not reach the compact object) will be

$$\begin{aligned} M_{\text{acc}} &= \frac{L_X t_X}{\eta c^2} \frac{\Omega}{4\pi} \\ &\approx 1.8 \frac{L_X}{10^{41} \text{ erg s}^{-1}} \frac{t_X}{10^5 \text{ yr}} \frac{0.01}{\eta} \frac{\Omega/4\pi}{0.1} M_{\odot}. \end{aligned} \quad (8)$$

By adopting  $\eta = 1\%$  in the second part of this expression, we crudely took into account the expected low radiative efficiency of supercritical accretion (e.g. Shakura & Sunyaev 1973; Jaroszynski, Abramowicz, & Paczynski 1980; Watarai et al. 2000; Poutanen et al. 2007) compared to standard, subcritical accretion ( $\sim 10\%$ ). Equation (9) implies that if a moderate,  $\Omega/4\pi \sim 0.1$ , degree of X-ray collimation is achieved, high luminosities  $L_X \lesssim 10^{41} \text{ erg s}^{-1}$  (note that for a power-law spectrum with  $\Gamma = 2.1$ ,  $L_X = 10^{41} \text{ erg s}^{-1}$  in our adopted 0.1–10 keV energy band corresponds to just  $\sim 3 \times 10^{40} \text{ erg s}^{-1}$  in the standard 2–10 keV X-ray band) can be sustained for a long time  $t_X \sim 10^5 \text{ yr}$  through the accretion of a reasonable amount of matter (few  $M_{\odot}$ ) from the companion (massive) star. These crude estimates are supported by detailed population synthesis studies of massive stellar binaries (Pavlovskii et al. 2017; Wiktorowicz et al. 2017).

### 3 ANALYTICAL ESTIMATES

Before proceeding to detailed numerical calculations, it is useful to obtain order-of-magnitude estimates for the ULX feedback on the ISM.

#### 3.1 Ionisation of hydrogen

Suppose first that the ISM consists purely of neutral hydrogen with constant number density  $n_{\text{H}}$  and temperature  $T_0 = 10^4 \text{ K}$ . In this case, the ULX, after switching on, will start inflating an HII zone. The radius of the latter will grow with time approximately (neglecting partial absorption of the ionising radiation within this radius) according to the differential equation  $\dot{N}_{\gamma}(1 + \langle N_s \rangle) dt = 4\pi n_{\text{H}} R_{\text{HII}}^2 dR_{\text{HII}}$ , where  $\dot{N}_{\gamma}$  is the apparent (i.e. isotropic-equivalent) number of hydrogen-photoionising ( $E > 13.6 \text{ eV}$ ) photons emitted by the ULX per second and  $\langle N_s \rangle$  is the average number of secondary ionisations induced by the primary photoelectron.

Hence,

$$R_{\text{HII}}(t) = \left[ \frac{3\dot{N}_{\gamma}(1 + \langle N_s \rangle)t}{4\pi n_{\text{H}}} \right]^{1/3}. \quad (9)$$

The maximum possible size of such an HII zone, determined by the balance between ionisations and recombinations, is given by the classical Strömgen formula:

$$R_{\text{HII,max}} = \left[ \frac{3\dot{N}_{\gamma}}{4\pi n_{\text{H}}^2 \alpha_{\text{HII}}} \right]^{1/3}, \quad (10)$$

where  $\alpha_{\text{HII}} \approx 2.54 \times 10^{-13} \text{ cm}^3 \text{ s}^{-1}$  is the Case B recombination rate for hydrogen at  $T = 10^4 \text{ K}$  (Draine 2011). Note that we have omitted the  $(1 + \langle N_s \rangle)$  factor in this expression, in contrast to equation (9), since a stationary HII zone is characterised by a high ionisation fraction (i.e. the fraction of free electrons)  $x_i \approx 1$ , so that secondary ionisations play a negligible role (the photoelectron deposits most of its energy into heat).

For our adopted X-ray spectrum (power-law with  $\Gamma = 2.1$  from 100 eV to 10 keV), all photons have energies above the hydrogen ionisation threshold, so that  $\dot{N}_{\gamma} \approx L_X/370 \text{ eV} \approx 1.7 \times 10^{50} (L_X/10^{41} \text{ erg s}^{-1}) \text{ s}^{-1}$  (here 370 eV is the ULX spectrum-weighted average energy of ionising photons). In a nearly neutral medium (with  $x_i < 0.01$ , as e.g. expected for a collisionally ionised ISM at  $T \sim 10^4 \text{ K}$ ), the fraction of the energy of the primary photoelectron (the latter being  $E - 13.6 \text{ eV} \approx E$ ) deposited into secondary ionisations is approximately constant,  $\sim 0.3$ , at energies above 100 eV (Furlanetto & Stoever 2010; Valdés & Ferrara 2008), so that  $\dot{N}_{\gamma}(1 + \langle N_s \rangle) \approx L_X/370 \text{ eV} + 0.3L_X/13.6 \text{ eV} \approx (0.17 + 1.38) \times 10^{51} (L_X/10^{41} \text{ erg s}^{-1}) \text{ s}^{-1} \approx 1.55 \times 10^{51} (L_X/10^{41} \text{ erg s}^{-1}) \text{ s}^{-1}$ . Hence,

$$R_{\text{HII}}(t) \approx 158 \left( \frac{L_X}{10^{41} \text{ erg s}^{-1}} \right)^{1/3} \left( \frac{t}{10^5 \text{ yr}} \right)^{1/3} \left( \frac{n_{\text{H}}}{10 \text{ cm}^{-3}} \right)^{-1/3} \text{ pc} \quad (11)$$

and

$$R_{\text{HII,max}} \approx 38 \left( \frac{L_X}{10^{41} \text{ erg s}^{-1}} \right)^{1/3} \left( \frac{n_{\text{H}}}{10 \text{ cm}^{-3}} \right)^{-2/3} \text{ pc}. \quad (12)$$

Therefore, to inflate the maximum possible HII zone ( $R_{\text{HII}} = R_{\text{HII,max}}$ ), the ULX must be active for a time longer than

$$t_{\text{HII}} \approx 1.4 \times 10^3 \left( \frac{n_{\text{H}}}{10 \text{ cm}^{-3}} \right)^{-1} \text{ yr}, \quad (13)$$

which does not depend on the ULX luminosity.

#### 3.2 Ionisation of helium

Despite the low abundance of helium compared to hydrogen in the ISM (their primordial number ratio is  $\sim 8$  to 92), a soft X-ray ( $E \sim 100\text{--}500 \text{ eV}$ ) photon emitted by the ULX is  $\sim 2$  times more likely to be absorbed by an HeI atom than by a HI atom. Therefore, the ULX might inflate a larger HeII zone compared to a HII zone.

Following the discussion for hydrogen above, the time-dependent and maximum sizes of the HeII zone can be estimated as

$$R_{\text{HeII}}(t) = \left[ \frac{3\dot{N}_{\gamma}(1 + \langle N_s \rangle)t}{4\pi n_{\text{H}}} \frac{n_{\text{H}}}{n_{\text{He}}} \right]^{1/3} \quad (14)$$

and

$$R_{\text{HeII,max}} = \left[ \frac{3\dot{N}_\gamma}{4\pi n_{\text{H}}^2 \alpha_{\text{HeII}}} \left( \frac{n_{\text{H}}}{n_{\text{He}}} \right)^2 \right]^{1/3}, \quad (15)$$

respectively, where  $\alpha_{\text{HeII}} \approx 2.72 \times 10^{-13} \text{ cm}^3 \text{ s}^{-1}$  is the case B recombination rate for helium at  $T = 10^4 \text{ K}$  (Draine 2011).

Compared to the case of hydrogen ionisation, the  $(1 + \langle N_s \rangle)$  factor plays a much less important role for helium, because the majority of secondary ionisations induced by the fast electron resulting from the photoionisation of a He atom will take place on H rather than He atoms. Specifically, in nearly neutral medium ( $x_i < 0.01$ ), the fraction of the energy of the photoelectron deposited into secondary ionisations of helium is  $\sim 0.025$  for energies  $\sim 100\text{--}500 \text{ eV}$  (Furlanetto & Stoever 2010)<sup>4</sup>. Therefore, given the HeI ionisation threshold of 24.6 eV,  $\dot{N}_\gamma(1 + \langle N_s \rangle) \approx L_X/370 \text{ eV} + 0.025 L_X/24.6 \text{ eV} \approx (1.7 + 0.6) \times 10^{50} (L_X/10^{41} \text{ erg s}^{-1}) \text{ s}^{-1} \approx 2.3 \times 10^{50} (L_X/10^{41} \text{ erg s}^{-1}) \text{ s}^{-1}$ , and thus

$$R_{\text{HeII}}(t) \approx 189 \left( \frac{L_X}{10^{41} \text{ erg s}^{-1}} \right)^{1/3} \left( \frac{t}{10^5 \text{ yr}} \right)^{1/3} \left( \frac{n_{\text{H}}}{10 \text{ cm}^{-3}} \right)^{-1/3} \text{ pc}; \quad (16)$$

$$R_{\text{HeII,max}} \approx 189 \left( \frac{L_X}{10^{41} \text{ erg s}^{-1}} \right)^{1/3} \left( \frac{n_{\text{H}}}{10 \text{ cm}^{-3}} \right)^{-2/3} \text{ pc}. \quad (17)$$

The maximum possible size of the HeII zone can be achieved in a time

$$t_{\text{HeII}} \approx 1.0 \times 10^5 \left( \frac{n_{\text{H}}}{10 \text{ cm}^{-3}} \right)^{-1} \text{ yr}. \quad (18)$$

Similar considerations can be applied to the case of a HeIII (fully ionised helium) zone. In this case, one can safely neglect the  $(1 + \langle N_s \rangle)$  factor, so that

$$R_{\text{HeIII}}(t) \approx 171 \left( \frac{L_X}{10^{41} \text{ erg s}^{-1}} \right)^{1/3} \left( \frac{t}{10^5 \text{ yr}} \right)^{1/3} \left( \frac{n_{\text{H}}}{10 \text{ cm}^{-3}} \right)^{-1/3} \text{ pc}; \quad (19)$$

$$R_{\text{HeIII,max}} \approx 94 \left( \frac{L_X}{10^{41} \text{ erg s}^{-1}} \right)^{1/3} \left( \frac{n_{\text{H}}}{10 \text{ cm}^{-3}} \right)^{-2/3} \text{ pc}; \quad (20)$$

$$t_{\text{HeIII}} \approx 1.7 \times 10^4 \left( \frac{n_{\text{H}}}{10 \text{ cm}^{-3}} \right)^{-1} \text{ yr}. \quad (21)$$

Here, we have taken into account the (relatively high) HeIII  $\rightarrow$  HeII recombination rate  $\alpha_{\text{HeIII}} \approx 2.19 \times 10^{-12} \text{ cm}^3 \text{ s}^{-1}$  at  $T = 10^4 \text{ K}$  (Draine 2011).

### 3.3 Preliminary conclusions and notes of caution

We can therefore draw the following preliminary conclusions: (i) a ULX can inflate a maximum-size ionisation zone within its lifetime ( $t_X \sim 10^5 \text{ yr}$ ) unless the typical ISM density  $n_{\text{H}} \ll 10 \text{ cm}^{-3}$ , (ii) the HII-zone is expected to be somewhat smaller compared to the HeII and HeIII zones, and (iii) for the most luminous ULXs ( $L_X \sim 10^{41} \text{ erg s}^{-1}$ ), the HeII/HeIII bubble can grow large enough ( $\sim 100 \text{ pc} \sim 0.1 R_{\text{vir}}$ ) to significantly [by  $\Delta N_{\text{H}} \sim 3 \times$

$10^{21} (L_X/10^{41} \text{ erg s}^{-1})^{1/3} (n_{\text{H}}/10 \text{ cm}^{-3})^{1/3} \text{ cm}^{-2}$ ] reduce the total X-ray absorption column density in front of the ULX, especially in smaller haloes.

In reality, the ionisation of hydrogen and helium will proceed in a joint fashion. Moreover, HeII  $\rightarrow$  HeIII ionisation follows HeI  $\rightarrow$  HeII ionisation, rather than proceeds simultaneously. Therefore, the estimates presented above in §3.1 and §3.2 should be taken with caution. Also, the above treatment in terms of classical Strömgren spheres may not be fully adequate for the problem at hand, since for typical soft X-ray energies playing a role here (50% and 90% of all photons have  $E < 200 \text{ eV}$  and  $E < 800 \text{ eV}$ , respectively), the photoionisation cross-section in a neutral H+He gas<sup>5</sup>  $\approx 6 \times 10^{-21} (E/200 \text{ eV})^{-3.2} \text{ cm}^{-2}$ , so that the photon mean free path is

$$\lambda \approx 5 \left( \frac{n_{\text{H}}}{10 \text{ cm}^{-3}} \right)^{-1} \left( \frac{E}{200 \text{ eV}} \right)^{3.2} \text{ pc}. \quad (22)$$

Therefore, the condition  $\lambda \ll (R_{\text{HII,max}}, R_{\text{HeII,max}}, R_{\text{HeIII,max}})$  will be fulfilled only if the gas is dense enough and/or the ULX is sufficiently luminous, namely if  $n_{\text{H}} \gg 0.1 (L_X/10^{41} \text{ erg s}^{-1})^{-1} \text{ cm}^{-3}$ . Otherwise, instead of a well-defined separation between a central ionised zone and the ambient nearly neutral gas, the ULX will cause a spatially distributed partial ionisation of the ISM.

Moreover, our assumption of an initially nearly neutral ISM may not be suitable for the host galaxies of ULXs in the early Universe. Indeed, a substantial fraction of the ISM may have temperatures significantly higher than  $10^4 \text{ K}$  in relatively massive ( $M \gtrsim 10^8 M_\odot$ ) haloes as a result of their virialisation (see equation 5), in which case collisional ionisation will lead to a non-negligible ionisation fraction  $x_i$ . In addition, the ISM may be pre-ionised by UV radiation and shock waves associated with star formation in the galaxy. All these processes, however, are unlikely to lead to a significant ionisation of helium in the ISM. Hence, our consideration of X-ray-driven helium ionisation should remain practically unaltered in this case.

### 3.4 ISM heating

The ULX radiation will not only ionise but also heat the surrounding ISM.

We may crudely estimate the amplitude of this effect using an ionisation parameter,  $U = \dot{N}_\gamma/4\pi R^2 n_{\text{H}} c$ <sup>6</sup>. Taking  $R \sim 100 \text{ pc}$  – the expected size of the ionisation zone, and given that  $\dot{N}_\gamma \approx 1.7 \times 10^{50} (L_X/10^{41} \text{ erg s}^{-1}) \text{ s}^{-1}$  for the adopted ULX spectrum, we find that  $U \sim 5 \times 10^{-4} (L_X/10^{41} \text{ erg s}^{-1}) (R/100 \text{ pc})^{-2} (n_{\text{H}}/10 \text{ cm}^{-3})^{-1}$ . As is well known (Draine 2011), for  $U \sim 10^{-5}\text{--}10^{-2}$ , the gas equilibrium temperature (determined by the balance between photoionisation heating and various cooling processes) is  $\sim (1-2) \times 10^4 \text{ K}$ . We may thus expect that even if the temperature of the ISM is initially lower than  $10^4 \text{ K}$ , the ULX will heat it to a few  $10^4 \text{ K}$  at distances  $\leq 100 \text{ pc}$ .

<sup>5</sup> This power-law dependence, derived from the more general and accurate formulae by Verner et al. 1996, is a good approximation at  $100 < E \leq 1000 \text{ eV}$ .

<sup>6</sup> In the considered case, the lower boundary of the spectral range, 100 eV, is higher than the ionisation threshold of hydrogen.

<sup>4</sup> Note that we have omitted the  $(1 + \langle N_s \rangle)$  factor in equation (15) for  $R_{\text{HeII,max}}$ , since even if the hydrogen remains mostly neutral, the HeII zone will be characterised by  $x_i > 0.1$ .

**Table 1.** Galaxy models

No.	$z$	$M$ ( $M_{\odot}$ )	$T_0/T_{\text{vir}}$	$T_0$ (K)	$R_{\text{vir}}$ (kpc)	$n_{\text{H}}(r=0)$ ( $\text{cm}^{-3}$ )
1	12.5	$10^7$	1	$5.8 \times 10^3$	0.52	2.3
2	10	$3 \times 10^7$	1	$9.9 \times 10^3$	0.91	1.2
3	10	$3 \times 10^7$	0.5	$4.9 \times 10^3$	0.91	15.4
4	10	$10^8$	0.5	$1.1 \times 10^4$	1.36	15.4
5	8	$3 \times 10^8$	0.5	$1.9 \times 10^4$	2.40	8.5
6	8	$3 \times 10^8$	0.25	$9.4 \times 10^3$	2.40	$1.25 \times 10^2$

We finally note that the sound-crossing time of the ionisation zone (with  $T \sim 10^4$  K) is expected to be  $\sim 100$  pc/10 km s $^{-1} \sim 10^7$  yr, much longer than the ionisation time (i.e. the ULX lifetime),  $t_{\text{X}} \lesssim 10^5$  yr. One can therefore consider the ionised gas to be stationary, despite it being over-pressured relative to the surrounding gas.

#### 4 NUMERICAL CALCULATIONS

To self-consistently compute the evolution of the expanding H/He ionisation region and the attenuation of the ULX emission by gas with the hydrostatic density distribution defined in §2.1 above, we took advantage of the publicly available numerical package CLOUDY (version 17.00), which makes it possible to perform photoionisation and radiative transfer computations in a time dependent manner (Ferland et al. 2017).

We start with defining several galaxy models (see Table 1) that may be regarded as representative examples in the context of the early X-ray heating of the Universe. To this end, we considered three reference epochs:  $z = 12.5$ , 10 and 8. Here, the first value is approximately the redshift when HMXBs probably became numerous enough to begin heating the IGM efficiently (e.g. Madau & Fragos 2017; Sazonov & Khabibullin 2017a),  $z \approx 8$  approximately marks the beginning of intense re-ionization of the Universe by UV radiation (so that X-ray heating becomes relatively unimportant), and  $z = 10$  may be considered a typical redshift of the X-ray heating epoch. Furthermore, this choice is convenient because the same redshifts were adopted as reference ones in the recent simulations of star formation in the early Universe by Xu et al. (2016), which largely governed our choice of fiducial galaxy masses below.

For  $z = 12.5$ , we considered a galaxy of total mass  $M = 10^7 M_{\odot}$ , since the bulk of star formation at this epoch was probably taking place in minihaloes with masses of this order. As typical star-forming galaxies were becoming more massive with decreasing redshift, we adopted  $M = 3 \times 10^7$  and  $10^8 M_{\odot}$  for  $z = 10$ , and  $M = 3 \times 10^8 M_{\odot}$  for  $z = 8$ . In reality, even more massive haloes,  $M \gtrsim 10^9 M_{\odot}$ , likely provided a significant contribution to the global SFR at  $z \lesssim 10$  (e.g. Xu et al. 2016), but we do not consider such galaxies in the present study since our adopted spherically symmetric gas density distribution (implying unrealistically high central densities for reasonable gas temperatures  $\sim 10^4$  K) is probably not a good approximation in this case owing to the likely formation of a central disc (e.g. Romano-Díaz et al. 2011; Pawlik, Milosavljević, & Bromm 2013).

The next parameter (see §2.1) is the initial gas temper-

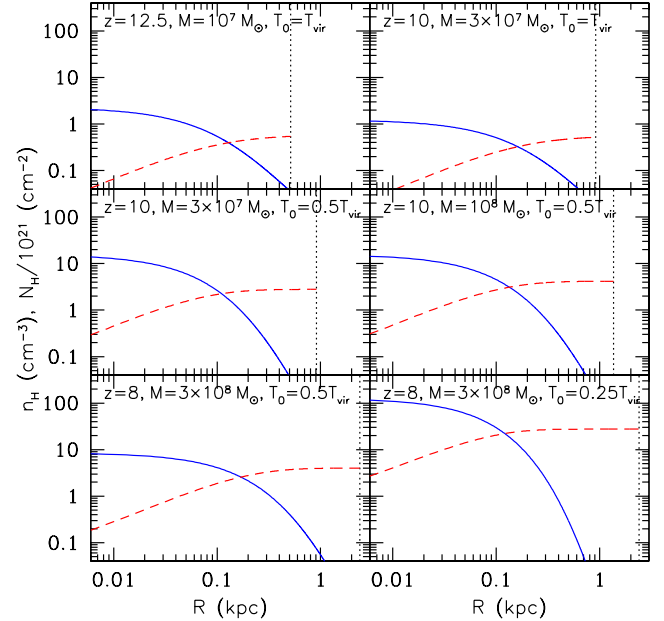


**Figure 1.** Hydrogen number density as a function of radius (blue solid lines) and column density within that radius (red dashed lines) for the galaxy models listed in Table 1 (the parameters of these models are also indicated in the panels). The vertical dotted lines denote the virial radii of the galaxies.

ature. Here, we adopted  $T_0 = T_{\text{vir}}$  for the  $M = 10^7 M_{\odot}$  minihalo and two alternative values,  $T_0 = T_{\text{vir}}$  and  $T_0 = 0.5T_{\text{vir}}$ , for the  $M = 3 \times 10^7 M_{\odot}$  halo. In these cases, the initial gas temperature is somewhat lower than  $10^4$  K, the temperature at which atomic cooling becomes efficient, and such regime is the defining property of minihaloes. By assuming  $T_0 = 0.5T_{\text{vir}}$ , we wish to explore how our results may change if the ISM has been able to significantly cool down (and hence to concentrate stronger toward the halo’s centre) upon virialisation. For our more massive galaxies, we adopted  $T_0 = 0.5T_{\text{vir}}$  and/or  $T_0 = 0.25T_{\text{vir}}$  (see Table 1), so that the initial gas temperature was always  $\sim 10^4$  K. We did not allow  $T_0 > 2 \times 10^4$  K, since atomic cooling is expected to quickly bring the ISM temperature down to  $\sim 10^4$  K upon virialisation should the virial temperature (i.e. the initial temperature of the shocked gas) be significantly higher. Fig. 1 shows the hydrogen number density radial profiles and the corresponding column densities for our galaxy models.

In reality, in those models with  $T_0 < 10^4$  K, we calculated the gas density profile by substituting  $T_0$  (as quoted in Table 1) into equation (6) but set the ISM temperature at  $10^4$  K at the onset of X-ray irradiation. This was done because: (i) CLOUDY is not well suited for low-temperature ( $T \lesssim 10^4$  K) regime and (ii) the ULX will quickly (within  $\sim 10^3$  years) heat up the ISM over the volume of interest to  $10^4$  K, since atomic cooling is inefficient at lower temperatures. We also note that the virial temperature ( $T_{\text{vir}}$ ) entering the above parametrisation in terms of  $T_0/T_{\text{vir}}$  was derived assuming a neutral medium, i.e.  $\mu = 1.2$  in equation (5), even if the actual initial (coronal-equilibrium) state of the ISM (as calculated by CLOUDY) was a significantly ionised one (as is the case for our hottest model with  $T_0 \approx 1.9 \times 10^4$  K).

We next adopted 5 fiducial values of the luminosity of the ULX:  $L_X = 10^{39.5}, 10^{40}, 10^{40.5}, 10^{41}$  and  $10^{41.5}$  erg s $^{-1}$ . Here, the luminosity is the bolometric one, for a spectrum given by

$$\frac{dN_\gamma}{dE} \propto E^{-2.1} e^{-100 \text{ eV}/E - E/10 \text{ keV}}, \quad (23)$$

which is slightly different from the power-law spectrum with sharp boundaries at 100 eV and 10 keV that we adopted for the analytical estimates in §3. Such a modification is supposed to render the numerical calculations better-behaved because of the absence of discontinuities in the spectrum of incident radiation.

For the spectrum given by equation (23), the fraction of the bolometric luminosity contained in the 0.1–10 keV and 0.25–8 keV bands (the latter was used in Sazonov & Khabibullin 2017b,c for construction of the X-ray luminosity function and collective X-ray spectrum of HMXBs in the local Universe) is 0.87 and 0.69, respectively.

We assumed the ISM to consist purely of hydrogen and helium, although we also ran a model with a non-negligible contribution of metals (at the level of 0.1 of the solar value, see §5.1 below). In both cases, molecular and grain physics were switched off by the corresponding options of the code. We adopted a spherical geometry with a density distribution given by equations (6) and (7) within  $R_{\text{vir}}$  (and no gas outside). The X-ray source was located at the center of the gas cloud.

The calculation starts with finding coronal equilibrium in the gas with uniform temperature  $T_0$ . After that, the ULX is switched on (at  $t = 0$ ) and allowed to shine at a constant luminosity  $L_X$  for a long time (specifically, we ran the computations up to  $t = 10^7$  yr), well in excess of realistic ULX lifetimes ( $\sim 10^5$  yr). As a result of illumination by the central source, the ionisation state, temperature and opacity of each shell evolve in time, and the code follows this evolution with the output produced at logarithmically spaced time steps.

At every iteration, we save physical conditions (temperature, H and He ionisation states etc.) across the whole computational domain along with the integrated energy-dependent optical depths and spectra of the radiation (the transmitted radiation of the central source and the radiation emitted by the photoionised gas) as it emerges at the outer boundary of the sphere. Comparing the properties of this emergent radiation with the intrinsic luminosity and spectrum of the central source, we manage to self-consistently track the evolution of the photoabsorption of X-rays from the ULX in its host galaxy.

## 5 RESULTS

Figures 2–8 show the results of our numerical calculations for a subsample of the considered galaxy/ULX models. Each figure shows the evolution of the radial profiles of the HI, HII, HeI, HeII and HeIII relative fractions, gas temperature and photoionisation optical depth, as well as the evolution of the transmitted X-ray spectrum. Specifically, the radial profiles and spectra are shown for elapsed times  $t = 0, 10^4, 10^5, 10^6$  and  $10^7$  years.

In the panels for hydrogen and helium, we also show analytical estimates of the radii of the HII and HeIII zones

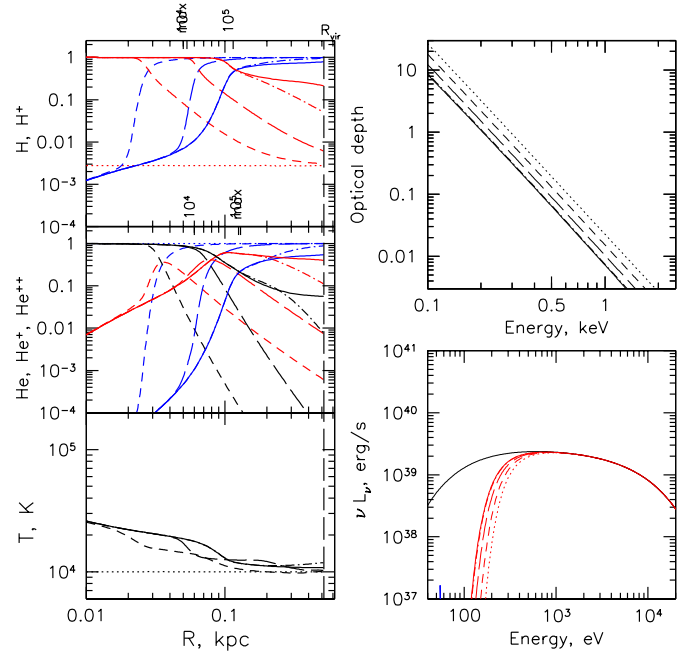


**Figure 2.** Results of computations for galaxy model 1 (see Table 1) and ULX luminosity  $L_X = 10^{40}$  erg s $^{-1}$ . *Top left:* Radial profiles of the HI and HII relative fractions (blue and red, respectively) as a function of time:  $t = 0$  (dotted),  $t = 10^4$  yr (short-dashed),  $t = 10^5$  yr (long-dashed),  $t = 10^6$  yr (dash-dotted) and  $t = 10^7$  yr (solid). The same line types are used in the other panels. Also shown (see the marks at the top of the panel) are the virial radius and the analytical estimates of the radius of the HII zone at  $t = 10^4, 10^5$  yr and in photoionisation equilibrium, given by eqs. (11) and (12), respectively. These were calculated for the  $n_H$  at the centre of the galaxy. *Middle left:* The same for the HeI (blue), HeII (red) and HeIII (black) relative fractions. The ticks at the top of the panel show the analytical estimates for  $R_{\text{HeIII}}$  at  $t = 10^4, 10^5$  yr and  $R_{\text{HeIII,max}}$  according to eqs. (19) and (20), respectively. *Bottom left:* Evolution of the gas temperature radial profile. *Top right:* Evolution of the photoionisation optical depth (as a function of energy). *Bottom right:* Evolution of the transmitted X-ray spectrum (red lines). The blue lines (if present) show the spectrum of the radiation emitted by the photoionised gas. The black line shows the intrinsic ULX spectrum.

based on the expressions presented in §3. To this end, we substituted the halo’s central hydrogen density (see the last column in Table 1) for  $n_H$ . We show  $R_{\text{HII}}$  and  $R_{\text{HeIII}}$  at  $t = 10^4$  and  $10^5$  yr, even if either radius becomes larger than the expected maximum size of the corresponding HeII or HeIII zone ( $R_{\text{HII,max}}$  and  $R_{\text{HeIII,max}}$ , respectively), i.e. even if  $t_{\text{HII}}$  or  $t_{\text{HeIII}}$  given by equations (13) and (21) prove to be shorter than  $10^4$  or  $10^5$  yr.

As expected, the less massive the galaxy is, the stronger is the impact of the ULX on the ISM. Consider first our least massive halo ( $M = 10^7 M_\odot, z = 12.5$ ), i.e. model 1 (see Table 1). As seen from Fig. 2, a ULX with a relatively low luminosity of  $10^{40}$  erg s $^{-1}$  can significantly (by a factor of  $\sim 2.5$ ) reduce the optical depth of the ISM within  $t \sim 10^5$  yr. As the photoionisation front propagates outwards, the affected ISM is heated up to  $\sim 2 \times 10^4$  K, which induces additional, collisional ionisation of the gas (in particular, hydrogen) and reduces its recombination rate. As a result, our analytical estimates

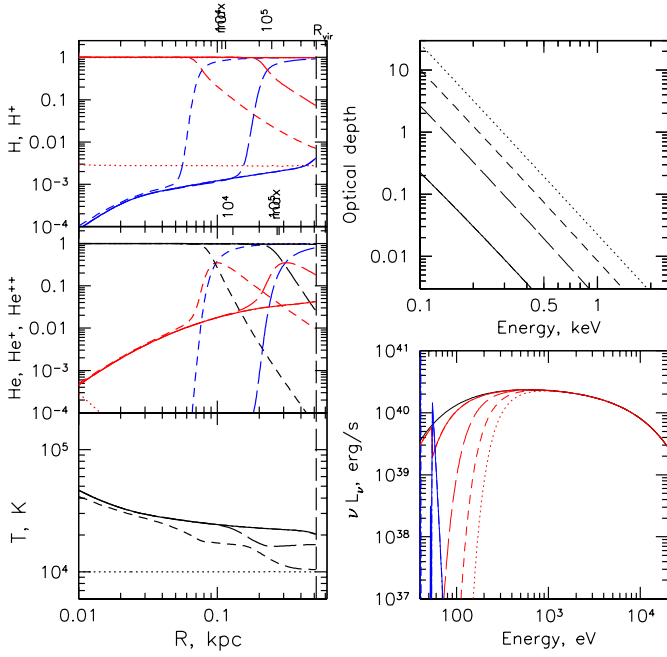


**Figure 3.** As Fig. 2, but for galaxy model 1 (see Table 1) and  $L_X = 10^{41}$  erg s $^{-1}$ .

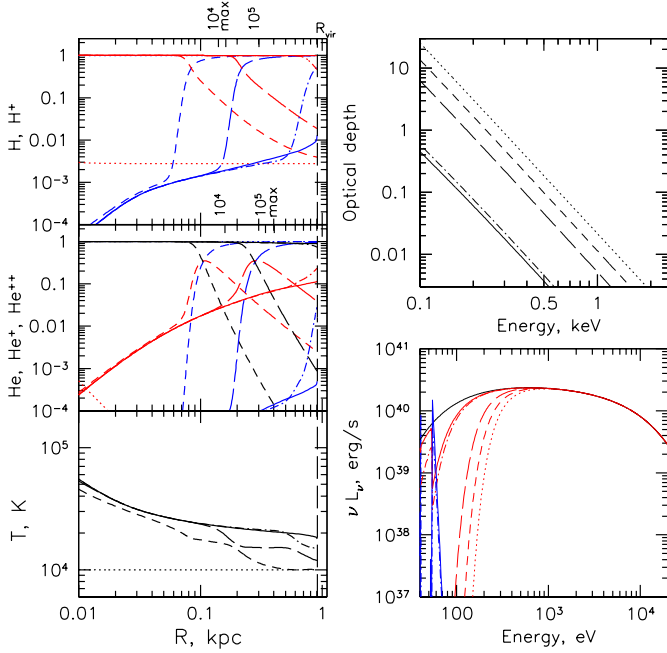


**Figure 4.** As Fig. 2, but for galaxy model 2 (see Table 1) and  $L_X = 10^{41}$  erg s $^{-1}$ .

(in §3) for the maximum size of the HII zone ( $R_{\text{HII,max}}$ ), derived under the assumption of photoionisation equilibrium at  $T = 10^4$  K, become inadequate, whereas our estimates for the time-dependent radii  $R_{\text{HII}}(t)$  and  $R_{\text{HeIII}}(t)$  as well as for the maximum size of the HeIII zone ( $R_{\text{HeIII,max}}$ ) prove to be fairly accurate (see Figs. 2–8). In the case of a more powerful ULX, with  $L_X = 10^{41}$  yr, the X-ray ionisation/heating effects become more dramatic: the optical depth drops by an

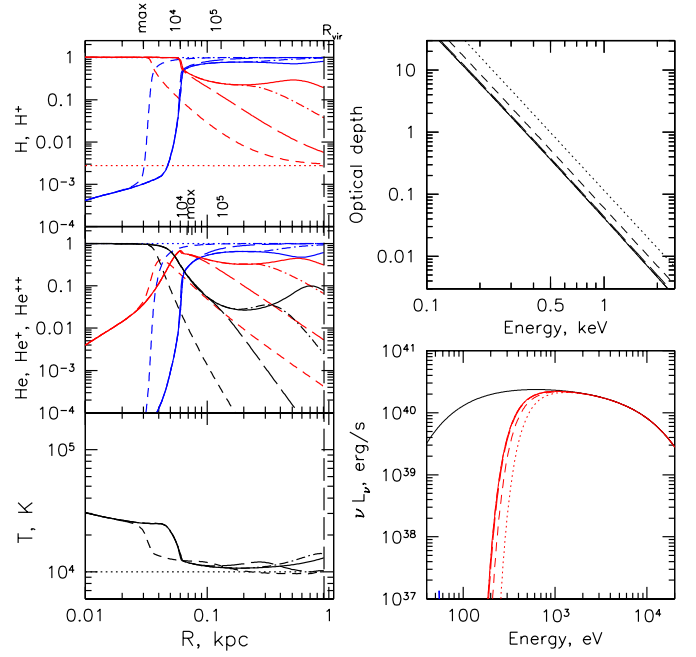


**Figure 5.** As Fig. 2, but for galaxy model 3 (see Table 1) and  $L_X = 10^{41}$  erg s $^{-1}$ .

order of magnitude within  $10^5$  yr, as most of the minihalo is ionised after this time (see Fig. 3).

Consider next a somewhat larger halo, as represented by our model 2 ( $M = 3 \times 10^7 M_\odot$ ,  $z = 10$ ). In this case, the virial temperature is  $9.9 \times 10^3$  K, at which atomic cooling is already important, so that this object may be considered a transitional case between minihaloes and dwarf galaxies. To make allowance for the uncertainty in the actual initial temperature and radial density distribution of the gas, we consider two cases,  $T_0 = T_{\text{vir}}$  and  $T_0 = 0.5T_{\text{vir}}$ . In the former case, as seen from Fig. 4, the ISM is ionised nearly as strongly as in the case of the  $10^7 M_\odot$  minihalo. Specifically, a ULX with  $L_X = 10^{41}$  erg s $^{-1}$  can reduce the total photoionisation optical depth by a factor of  $\sim 5$  after  $t \sim 10^5$  yr. The ionisation effect becomes less dramatic in the  $T_0 = 0.5T_{\text{vir}}$  case (see Fig. 5), since the central gas density is now an order of magnitude higher than for  $T_0 = T_{\text{vir}}$  ( $n_{\text{H}} = 15.4$  vs.  $1.2$  cm $^{-3}$ ) and it is more difficult for the ULX to ionise and heat the central regions of the halo.

For the yet more massive halo represented by our model 4 ( $M = 10^8 M_\odot$ ,  $z = 10$ ), the ionisation effect is still noticeable: a ULX with  $L_X = 10^{41}$  erg s $^{-1}$  can reduce the total photoionisation optical depth by a factor of  $\sim 2$  after  $t \sim 10^5$  yr (see Fig. 6). However, our most massive galaxy ( $M = 3 \times 10^8 M_\odot$ ,  $z = 8$ ) is almost unaffected by X-ray irradiation (see Figs. 7 and 8), regardless of the actual configuration of the gas (compare the results for model 5 with  $T_0 = 0.5T_{\text{vir}} = 1.9 \times 10^4$  K and model 6 with  $T_0 = 0.25T_{\text{vir}} = 9.4 \times 10^3$  K). In the latest (densest) case, the ionisation front is unable to propagate further out than  $\sim 10$  pc, although X-ray photons of relatively high energy ( $E \gtrsim 1$  keV) are able to propagate to large distances from the ULX and eventually raise the ionisation fraction (i.e. the relative fractions of HII and HeII) to a few per cent over the bulk of the galaxy.

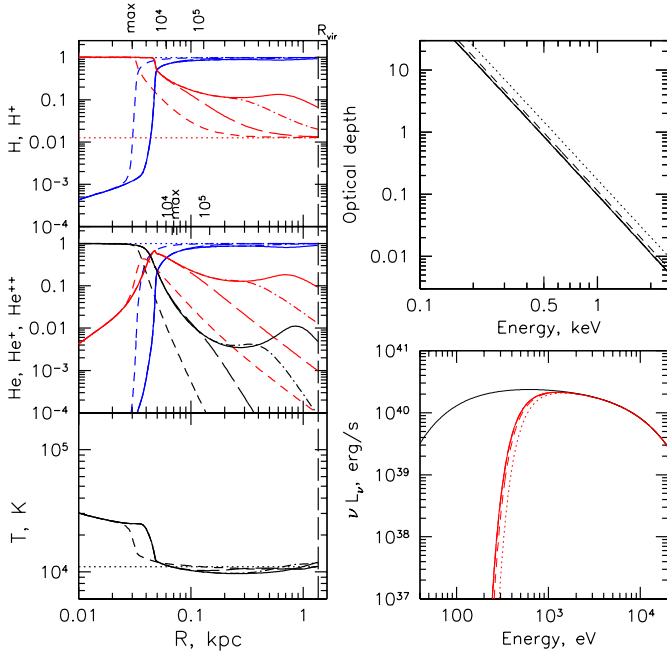


**Figure 6.** As Fig. 2, but for galaxy model 4 (see Table 1) and  $L_X = 10^{41}$  erg s $^{-1}$ .

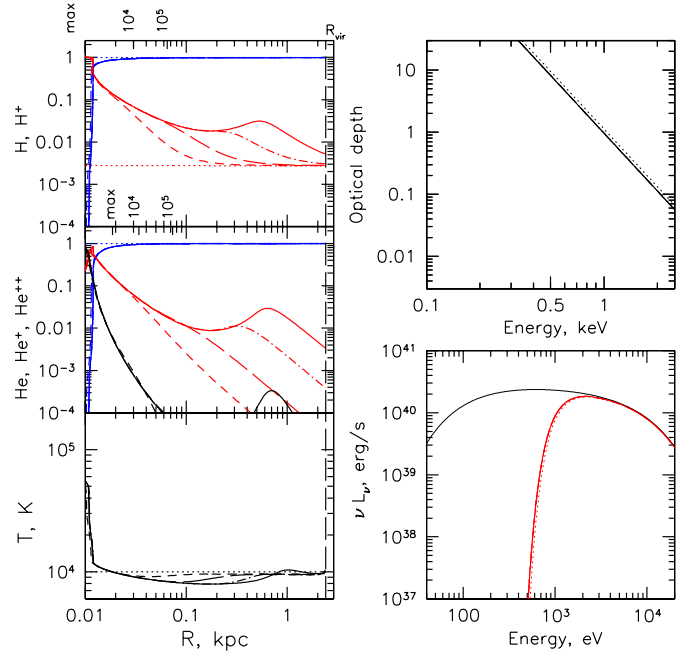


**Figure 8.** As Fig. 2, but for galaxy model 6 (see Table 1) and  $L_X = 10^{41}$  erg s $^{-1}$ .

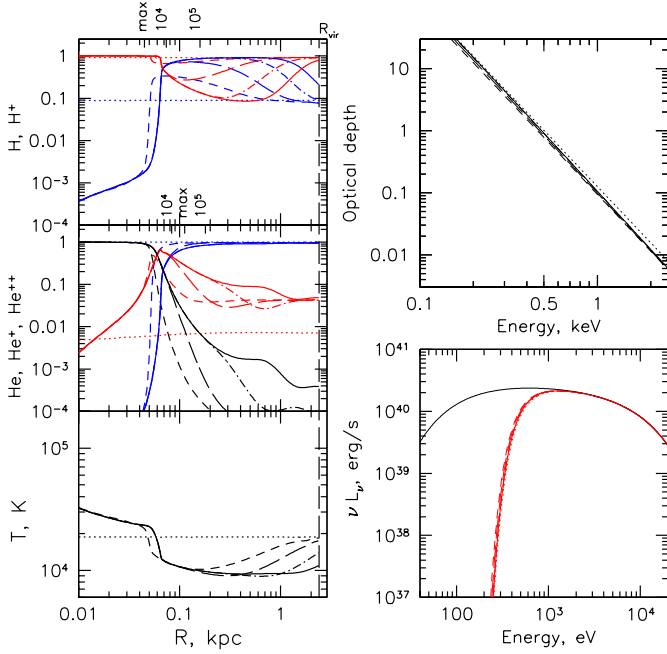


**Figure 7.** As Fig. 2, but for galaxy model 5 (see Table 1) and  $L_X = 10^{41}$  erg s $^{-1}$ .

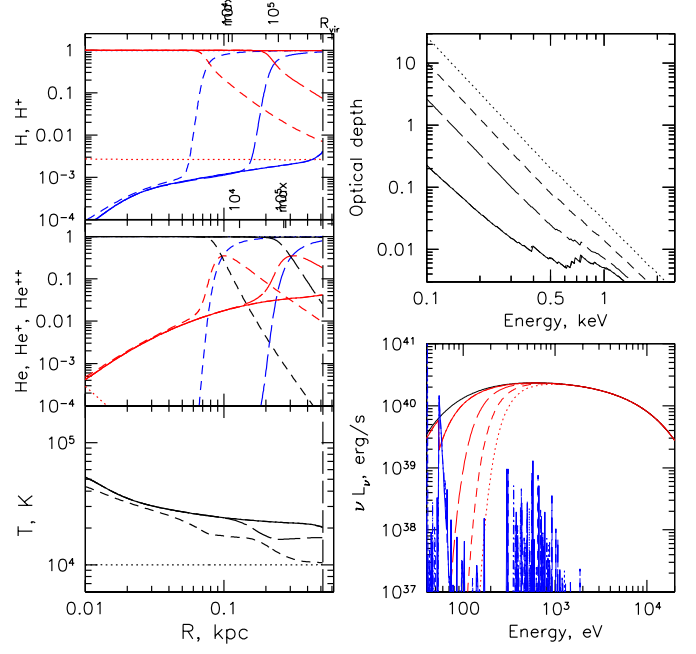


**Figure 9.** As Fig. 3 (galaxy model 1 and  $L_X = 10^{41}$  erg s $^{-1}$ ), but for non-zero metallicity  $Z = 0.1$ .

### 5.1 Impact of metal enrichment

The ISM at  $z \sim 10$  may have already been weakly (to less than a few per cent of the solar metallicity, e.g. Pallottini et al. 2014) enriched by metals. We have therefore repeated the computations for some of our models adding a  $Z = 0.1$  (with respect to the solar abundances) fraction of heavy elements to the primordial mixture of hydrogen and helium.

Figure 9 shows an example of such a test. By comparing these plots with those for the same galaxy/ULX model but without metals (Fig. 3), we see that the results have remained almost unaltered. A difference is only noticeable at energies above  $\sim 500$  eV, where the metals (mainly oxygen and the L-shell of iron) start to contribute significantly to the optical depth of the ISM once the hydrogen and helium have been photoionised by the ULX. However, since the ISM

optical depth at these energies is already very small by this moment, the overall difference in the transmitted soft X-ray flux (see below) between the metal-poor and metal-free cases is not significant.

## 5.2 Ultimate effect on the transmitted X-ray flux

The bottom right panels of Figs. 2–8 show the X-ray spectrum emergent from the galaxy at different times ( $t = 0, 10^4, 10^5, 10^6$  and  $10^7$  yr). These spectra represent the ULX radiation transmitted through the ISM. The contribution of the emission produced by the ISM itself (also shown in the figures) is negligible in the considered energy range ( $\gtrsim 50$  eV), since the gas always remains colder than  $\sim 7 \times 10^4$  K.

As scattering on free electrons provides a negligible contribution to the total optical depth through the gas, the emergent X-ray spectrum is approximately equal to the incident spectrum [given by eq. (23)] multiplied by  $\exp[-\tau(E)]$ , where  $\tau(E)$  is the photoabsorption optical depth, plotted in the top right panels of Figs. 2–8. For the problem of X-ray heating of the IGM in the early Universe, the most interesting property of a population of X-ray sources (e.g. HMXBs), apart from its cumulative luminosity, is the fraction of the intrinsic soft X-ray (below  $\sim 1$  keV) luminosity escaping from the host galaxies. Note that because the IGM remains nearly neutral during the X-ray heating epoch, it is mainly the soft X-ray luminosity rather than the total number of soft X-ray photons that is of importance, since secondary ionisations caused by fast photoelectrons play a major role. This is in contrast to X-ray irradiation of the ISM within galaxies, where the gas eventually becomes significantly ionised so that harder X-ray photons release most of their energy as heat rather than in multiple ionisations.

Therefore, we determined for all of our galaxy/ULX models the ratio  $R_{\text{SX}} \equiv L_{\text{SX,esc}}/L_{\text{SX}}$ , where  $L_{\text{SX}}$  is the intrinsic luminosity of the ULX in the soft X-ray (0.1–1 keV) energy band (note that  $L_{\text{SX}}/L_X = 0.48$  for our adopted ULX spectrum) and  $L_{\text{SX,esc}}$  is the transmitted luminosity in the same band. This ratio is shown in Fig. 10 for the sampled galaxy/ULX models and different elapsed times.

We see that for the  $M = 10^7 M_\odot$  minihalo,  $R_{\text{SX}} \approx 50\%$  at the start of X-ray irradiation ( $t = 0$ ), and the ULX, depending on its luminosity ( $L_X = 10^{39.5} - 10^{41.5}$  erg s $^{-1}$ ), gradually increases the escape fraction to  $\sim 60$ –100% within  $t = 10^5$  yr. For our somewhat larger halo ( $M = 3 \times 10^7 M_\odot$ ) and  $T_0 = T_{\text{vir}} = 9.9 \times 10^3$  K, the impact of the ULX on  $R_{\text{SX}}$  is somewhat weaker, and it weakens further (but remains significant) if the gas configuration is more compact ( $T_0 = 0.5T_{\text{vir}}$ ). For the more massive halo with  $M = 10^8 M_\odot$  (and  $T_0 = 0.5T_{\text{vir}}$ ), a ULX with  $L_X = 10^{41}$  erg s $^{-1}$  can increase  $R_{\text{SX}}$  from  $\approx 20\%$  to  $\approx 30\%$  within  $10^5$  yr. Finally, for our most massive halo ( $M = 3 \times 10^8 M_\odot$ ), X-ray irradiation is unable to significantly affect the transmitted soft X-ray flux for realistic ULX luminosities ( $L_X \lesssim$  a few  $10^{41}$  erg s $^{-1}$ )<sup>7</sup>.

In reality, X-ray heating is not expected to be homogeneous in the early Universe, as the IGM in the close vicinity of strong X-ray sources might be heated to somewhat higher

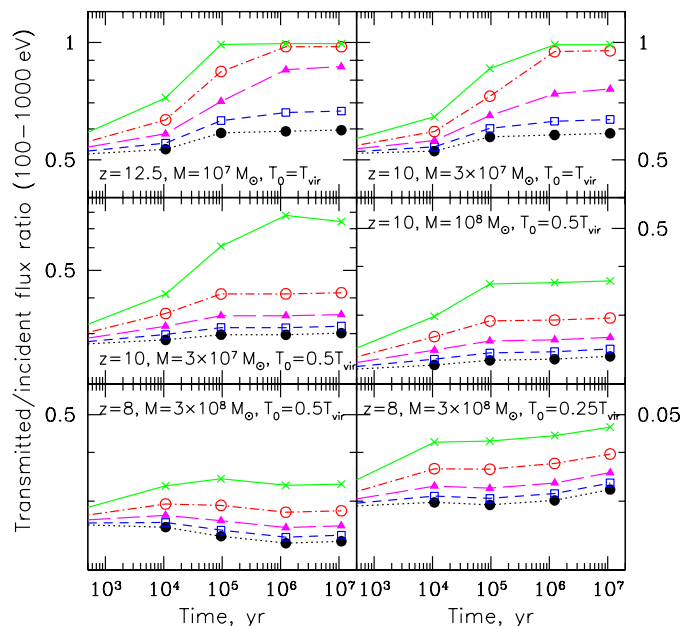


**Figure 10.** Fraction of the soft X-ray (0.1–1 keV) luminosity of the ULX transmitted through the galaxy as a function of time elapsed since the switch-on of the source, for the different galaxy models (see Table 1 and the labels inside the panels), as a function of the bolometric luminosity of the ULX:  $L_X = 10^{39.5}$  erg s $^{-1}$  (black filled circles connected by the dotted line),  $L_X = 10^{40}$  erg s $^{-1}$  (blue open squares connected by the short-dashed line),  $L_X = 10^{40.5}$  erg s $^{-1}$  (magenta filled triangles connected by the long-dashed line),  $L_X = 10^{41}$  erg s $^{-1}$  (red open circles connected by the dash-dotted line) and  $L_X = 10^{41.5}$  erg s $^{-1}$  (green crosses connected by the solid line). Note the different vertical scales for different models.

temperatures than elsewhere. Since the mean free path of X-ray photons increases dramatically with increasing photon energy,  $\bar{\lambda} \sim 5[(1+z)/10]^{-3}(E/500 \text{ eV})^{3.2}$  proper Mpc (e.g. Sazonov & Khabibullin 2017a), it is only the softest photons that can play a role in such localised heating. It is thus interesting to additionally evaluate the escape fraction for the supersoft (100–300 eV) energy band:  $R_{\text{SSX}} \equiv L_{\text{SSX,esc}}/L_{\text{SSX}}$ , where  $L_{\text{SSX}}$  and  $L_{\text{SSX,esc}}$  are the intrinsic and transmitted ULX luminosities in this band (note that  $L_{\text{SSX}}/L_X = 0.20$  for our adopted ULX spectrum). The resulting dependences of  $R_{\text{SSX}}$  on  $L_X$  and  $t$  for the different galaxy models are shown in Fig. 11.

As could be expected, the impact of the ULX on the escape fraction is much more dramatic in the supersoft band. The  $R_{\text{SSX}}$  fraction increases noticeably as a result of X-ray irradiation for all of our galaxy models. It should be noted, however, that for the more massive haloes ( $M = 10^8 M_\odot$  and  $3 \times 10^8 M_\odot$ ), the supersoft X-ray escape fraction remains below 1% even for the most luminous ULXs (in particular,  $R_{\text{SSX}} \approx 0$  for Model 6, due to the huge optical depth). Therefore, soft X-rays from ULXs may cause a significant extra heating of the IGM only near minihaloes and dwarf galaxies with  $M \lesssim$  a few  $\times 10^7 M_\odot$ .

<sup>7</sup> Note that for model 5,  $R_{\text{SX}}$  actually decreases with time for  $L_X \lesssim 10^{41}$  erg s $^{-1}$ , due to the ISM cooling to  $\sim 10^4$  K from its initial (relatively high) temperature of  $1.9 \times 10^4$  K.

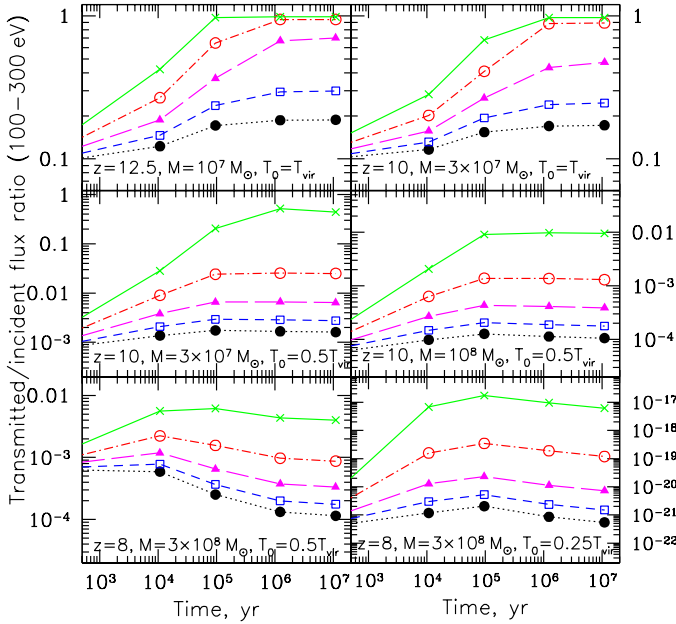


**Figure 11.** The same as Fig. 10, but for the supersoft (100–300 eV) energy band.

## 6 DISCUSSION

This study is just a first step in the exploration of the potential impact of ULXs/HMXBs on the X-ray opacity of their host dwarf galaxies and minihaloes in the early Universe. The galaxy models considered in this paper are admittedly over-simplified, not least because direct observations of the first galaxies will not become possible until the next generation of ground-based and satellite-borne telescopes come into operation.

The main assumption of our current model is that the ISM is in single-temperature hydrostatic equilibrium in the dark matter potential well. As demonstrated by detailed simulations (e.g. Wise et al. 2014; Das et al. 2017; Trebitsch et al. 2017), the actual gas distribution is likely to be substantially inhomogeneous, so that gas column densities may vary greatly from one viewing direction to another for a given galaxy. This implies that if such a galaxy hosts a luminous X-ray source, its radiation will preferentially escape through low-density channels in the ISM, and this anisotropic escape will be strengthened by feedback of the ULX on the ISM, since it is easier for X-rays to ionise and heat a rarefied medium.

The X-ray mode of feedback discussed in this paper may well work in concert with other types of back-reaction associated with star formation, such as mechanical feedback (through winds and collimated outflows) from X-ray binaries, including the ULXs responsible for the X-ray feedback (e.g. Justham & Schawinski 2012), as well as radiative and mechanical feedback from massive stars and supernovae. In principle, the starburst episode associated with the appearance of a ULX could rarefy, pre-ionise and heat the gas in the galaxy, helping the ULX to ionise it (within the X-ray beam) more strongly afterwards. However, the actual se-

quence of events is not well known. In particular, since the majority of ULXs in the first galaxies were probably among the highest-mass, and hence most rapidly evolving, stellar binaries, they could inject their energy into the ISM before luminous supernovae started to provide a substantial feedback. Moreover, the relative importance of stellar and ULX feedback in the early Universe may have varied greatly from one dwarf galaxy to another, since the latter is dominated by the brightest, and hence very rare, ULXs (see §1). We refer the reader to the papers by Justham & Schawinski (2012); Artale, Tissera, & Pellizza (2015) for a detailed discussion of these issues.

Clearly, in order to more realistically evaluate the escape fraction of soft X-rays from ULXs in the early Universe, it is necessary to include the X-ray feedback described in this paper into detailed simulations of star formation in the first galaxies together with all other relevant physical processes. Moreover, the present study is effectively limited to haloes with masses below  $\sim 3 \times 10^8 M_\odot$ . More massive galaxies are likely to have central discs, and the propagation of X-rays from ULXs located inside such discs requires a separate investigation.

As was explained in the introduction (§1), only a tiny fraction ( $\lesssim 1\%$ ) of galaxies in the early Universe are expected to host a ULX with  $L_X \gtrsim 10^{40}$  erg s $^{-1}$  at a given moment. However, assuming that such X-ray sources remain active for a time ( $t_X \sim 10^5$  yr) that is much shorter than the duration of the corresponding starburst episode,  $t_{sf} \sim 10^7$ – $10^8$  yr, there is nevertheless a significant probability that a typical galaxy at  $z \sim 10$  will host one or even a few bright ULXs over the whole history of its star formation activity. It is unlikely though that several ULXs appearing in the same galaxy will lead to a larger fraction of their X-ray emission escaping into the IGM, since their ionisation bubbles will be largely independent of each other (due to random directions of the X-ray beams and the time span between the bubbles being much longer than the characteristic recombination time of the ISM).

In this connection, it is also worth noting that a typical galaxy in the early Universe would exhibit only relatively low-luminosity HMXBs at a given time. Indeed, given the HMXB LF measured in the local Universe (Mineo, Gilfanov, & Sunyaev 2012; Sazonov & Khabibullin 2017b) and assuming (perhaps optimistically) that the specific occurrence rate of HMXBs was a factor of  $\sim 10$  higher at  $z \sim 10$ , a typical galaxy at that epoch, with a SFR  $\lesssim 0.01 M_\odot$  yr $^{-1}$ , is not expected to have HMXBs with  $L_X > \text{a few} \times 10^{37}$  erg s $^{-1}$  at a given instant. The combined luminosity of such sources is therefore less than  $10^{38}$  erg s $^{-1}$ . Based on the results of the present study, it is clear that such low-luminosity HMXBs should have virtually no impact on the ISM of their host galaxy.

It is also worth noting that although the present study was devoted to the particular case of ULXs, its results may also be interesting in considering other types of X-ray sources that could heat the IGM in the early stages of cosmic re-ionisation, such as growing supermassive black holes (i.e. microquasars, see e.g. Madau et al. 2004; Ricotti & Ostriker 2004; Wyithe & Loeb 2004; Thomas & Zaroubi 2008). Since in this case more luminous and more prolonged (compared to ULXs) episodes of X-ray activity are possible, one may get an idea of the expected impact on the ISM (and

hence on the transmitted soft X-ray flux fraction) by looking at the results of our computations for the maximum considered values of the X-ray source parameters, namely  $L_X \sim$  a few  $10^{41}$  erg s $^{-1}$  and  $t \sim 10^6$ – $10^7$  yr (see Figs. 10 and 11).

## 7 SUMMARY

If the analogy with the local Universe is correct, then ULXs with (isotropic-equivalent) luminosity  $L_X \gtrsim 10^{40}$  erg s $^{-1}$  are expected to provide the bulk of the X-ray emission associated with star formation in the early Universe. We have evaluated the photoionisation effect of such strong individual X-ray sources on the ISM of their host galaxies.

We found that ULXs with  $L_X \gtrsim 10^{40}$ – $10^{41}$  erg s $^{-1}$  (0.1–10 keV) can significantly ionise the ISM (in particular, helium), and thus reduce its opacity to soft X-rays, in minihaloes and dwarf galaxies with total masses  $M \sim 10^7$ – $10^8 M_\odot$  at  $z \gtrsim 10$  provided that the X-ray source remains active for a  $t_X \sim 10^5$  yr, which, according to recent population synthesis studies of HMXBs, is not an unreasonably long time for a supercritical accretion phase onto a neutron star or a stellar-mass black hole. As a result, the fraction of the soft X-ray (0.1–1 keV) luminosity escaping from a galaxy hosting a bright ULX can increase from  $\sim 20$ – $50\%$  to  $\sim 30$ – $80\%$  (depending on  $M$  and  $L_X$ ) over the ULX lifetime. This implies that ULXs (and hence HMXBs as a whole) can induce a stronger heating of the IGM in the early Universe compared to estimates neglecting X-ray feedback.

ULX feedback is even more efficient in the supersoft X-ray energy range (100–300 eV), with the escape fraction in this band increasing several times as a result of X-ray irradiation of the ISM by a ULX. This may allow ULXs located in minihaloes and dwarf galaxies at  $z \gtrsim 10$  to significantly heat the IGM in their vicinity.

On the other hand, we have shown that larger galaxies with  $M \gtrsim 3 \times 10^8 M_\odot$  could not be significantly ionised even by the brightest ULXs in the early Universe. Since such galaxies probably started to dominate the global SFR at  $z \lesssim 10$ , the overall escape fraction of soft X-rays from the HMXB population probably remained low,  $\lesssim 30\%$ , at these epochs.

## ACKNOWLEDGMENTS

The research was supported by the Russian Science Foundation (grant 14-12-01315).

## REFERENCES

Artale M. C., Tissera P. B., Pellizza L. J., 2015, *MNRAS*, 448, 3071  
 Basu-Zych A. R., Lehmer B., Fragos T., Hornschemeier A., Yukita M., Zezas A., Ptak A., 2016, *ApJ*, 818, 140  
 Begelman M. C., King A. R., Pringle J. E., 2006, *MNRAS*, 370, 399  
 Berghea C. T., Dudik R. P., Weaver K. A., Kallman T. R., 2010, *ApJ*, 708, 364  
 Bertschinger E., 1985, *ApJS*, 58, 39  
 Brorby M., Kaaret P., Prestwich A., 2014, *MNRAS*, 441, 2346  
 Cherepashchuk A. M., Aslanov A. A., Kornilov V. G., 1982, *SvA*, 26, 697

Cohen A., Fialkov A., Barkana R., Lotem M., 2017, *MNRAS*, 472, 1915  
 Das A., Mesinger A., Pallottini A., Ferrara A., Wise J. H., 2017, *MNRAS*, 469, 1166  
 Dolan J. F., et al., 1997, *A&A*, 327, 648  
 Douma V. M., Pellizza L. J., Mirabel I. F., Pedrosa S. E., 2015, *A&A*, 579, A44  
 Douma V. M., Pellizza L. J., Laurent P., Mirabel I. F., 2017, arXiv:1711.07374  
 Draine B. T., 2011, *piim.book*  
 Fabrika S., 2004, *ASPRv*, 12, 1  
 Fabrika S., Mescheryakov A., 2001, *IAUS*, 205, 268  
 Fabrika S., Ueda Y., Vinokurov A., Sholukhova O., Shidatsu M., 2015, *NatPh*, 11, 551  
 Ferland G. J., et al., 2017, *RMxAA*, 53, 385  
 Ferrara A., Loeb A., 2013, *MNRAS*, 431, 2826  
 Furlanetto S. R., Stoeber S. J., 2010, *MNRAS*, 404, 1869  
 Greif T. H., Johnson J. L., Klessen R. S., Bromm V., 2008, *MNRAS*, 387, 1021  
 Jaroszynski M., Abramowicz M. A., Paczynski B., 1980, *AcA*, 30, 1  
 Justham S., Schawinski K., 2012, *MNRAS*, 423, 1641  
 Kaaret P., Ward M. J., Zezas A., 2004, *MNRAS*, 351, L83  
 Kaaret P., Feng H., Roberts T. P., 2017, *ARA&A*, 55, 303  
 Kawashima T., Ohsuga K., Mineshige S., Yoshida T., Heinzeller D., Matsumoto R., 2012, *ApJ*, 752, 18  
 Khabibullin I., Sazonov S., 2016, *MNRAS*, 457, 3963  
 King A. R., 2009, *MNRAS*, 393, L41  
 Lehmer B. D., et al., 2016, *ApJ*, 825, 7  
 Leite N., Evoli C., D’Angelo M., Ciardi B., Sigl G., Ferrara A., 2017, *MNRAS*, 469, 416  
 Loeb A., Furlanetto S. R., 2013, *The First Galaxies in the Universe*, by Abraham Loeb and Steven R. Furlanetto. Princeton University Press  
 Madau P., Rees M. J., Volonteri M., Haardt F., Oh S. P., 2004, *ApJ*, 604, 484  
 Madau P., Fragos T., 2017, *ApJ*, 840, 39  
 Makino N., Sasaki S., Suto Y., 1998, *ApJ*, 497, 555  
 Medvedev P., Sazonov S., Gilfanov M., 2016, *MNRAS*, 459, 431  
 Mirabel I. F., Dijkstra M., Laurent P., Loeb A., Pritchard J. R., 2011, *A&A*, 528, A149  
 Mineo S., Gilfanov M., Sunyaev R., 2012, *MNRAS*, 419, 2095  
 Narayan R., Sądowski A., Soria R., 2017, *MNRAS*, 469, 2997  
 Navarro J. F., Frenk C. S., White S. D. M., 1997, *ApJ*, 490, 493  
 Nielsen M. T. B., Gilfanov M., 2015, *MNRAS*, 453, 2927  
 Pakull M. W., Mirioni L., 2003, *RMxAC*, 15, 197  
 Pallottini A., Ferrara A., Gallerani S., Salvadori S., D’Odorico V., 2014, *MNRAS*, 440, 2498  
 Pavlovskii K., Ivanova N., Belczynski K., Van K. X., 2017, *MNRAS*, 465, 2092  
 Pawlik A. H., Milosavljević M., Bromm V., 2013, *ApJ*, 767, 59  
 Pilipenko S. V., Sánchez-Conde M. A., Prada F., Yepes G., 2017, *MNRAS*, 472, 4918  
 Poutanen J., Lipunova G., Fabrika S., Butkevich A. G., Abolmasov P., 2007, *MNRAS*, 377, 1187  
 Rappaport S. A., Podsiadlowski P., Pfahl E., 2005, *MNRAS*, 356, 401  
 Ricotti M., Ostriker J. P., 2004, *MNRAS*, 352, 547  
 Romano-Díaz E., Choi J.-H., Shlosman I., Trenti M., 2011, *ApJ*, 738, L19  
 Ross H. E., Dixon K. L., Iliev I. T., Mellema G., 2017, *MNRAS*, 468, 3785  
 Sazonov S., Khabibullin I., 2017a, *Astron. Lett.*, 43, 243  
 Sazonov S., Khabibullin I., 2017b, *MNRAS*, 466, 1019  
 Sazonov S., Khabibullin I., 2017c, *MNRAS*, 468, 2249  
 Sazonov S., Sunyaev R., 2015, *MNRAS*, 454, 3464  
 Shakura N. I., Sunyaev R. A., 1973, *A&A*, 24, 337  
 Thomas R. M., Zaroubi S., 2008, *MNRAS*, 384, 1080

- Trebitsch M., Blaizot J., Rosdahl J., Devriendt J., Slyz A., 2017, MNRAS, 470, 224
- Tueros M., del Valle M. V., Romero G. E., 2014, A&A, 570, L3
- Valdés M., Ferrara A., 2008, MNRAS, 387, L8
- Venkatesan A., Giroux M. L., Shull J. M., 2001, ApJ, 563, 1
- Verner D. A., Ferland G. J., Korista K. T., Yakovlev D. G., 1996, ApJ, 465, 487
- Vinokurov A., Fabrika S., Atapin K., 2013, AstBu, 68, 139
- Watarai K.-y., Fukue J., Takeuchi M., Mineshige S., 2000, PASJ, 52, 133
- Wiktorowicz G., Sobolewska M., Lasota J.-P., Belczynski K., 2017, ApJ, 846, 17
- Wise J. H., Abel T., 2007, ApJ, 665, 899
- Wise J. H., Cen R., 2009, ApJ, 693, 984
- Wise J. H., Demchenko V. G., Halicek M. T., Norman M. L., Turk M. J., Abel T., Smith B. D., 2014, MNRAS, 442, 2560
- Wyithe J. S. B., Loeb A., 2004, ApJ, 610, 117
- Xu Y., Ferrara A., Chen X., 2011, MNRAS, 410, 2025
- Xu H., Wise J. H., Norman M. L., Ahn K., O’Shea B. W., 2016, ApJ, 833, 84

This paper has been typeset from a  $\text{\TeX}/\text{\LaTeX}$  file prepared by the author.